ROYAL SOCIETY OF CHEMISTRY

PAPER

Check for updates

How a quantum computer could accurately solve a hydrogen-air combustion model†

Alejandro Becerra,[abc] Oscar Homero Diaz-Ibarra,[d] Kyungjoo Kim,[d] Bert Debusschere [ID][d] and Eric A. Walker [ID] *[ef]

A quantum circuit method for modeling steady state behavior of homogeneous hydrogen-air combustion is presented. Extensive empirical testing has pinpointed the factor determining accuracy of quantum circuit calculations. Specifically, the accuracy of the Harrow, Hassidim and Lloyd (HHL) algorithm has been benchmarked using Qiskit simulations. For random linear systems that were constricted by various criteria, the quantum solution was compared to the classical solution. The criteria investigated include orthogonality, condition number, orthonormality, angle between vectors within the linear system, diagonality, and the angle between the solution vector and the right-hand side (RHS) vector. The results of these rigorous tests show that the single most powerful factor in accuracy is the angle between the solution vector and the RHS vector. This insight was used to inform the preconditioning of two reduced models of hydrogen-air combustion. These models have been compared in terms of accuracy and degree of utility in terms of the physical system. This application area could exploit a quantum advantage *via* the poly-logarithmic scaling of HHL.

Introduction

Currently, there is a great amount of interest in developing quantum computers, especially hardware and algorithms.[1] Encryption[2] and electronic structures of molecules are of particular interest because a quantum advantage has been shown in principle. Another area of research is quantum machine learning.[3]

Mansouri, *et al.*,[4] the authors of which have a start-up company affiliation, have published their perspective on the possible chemical industrial application of quantum computers. The perspective was on making chemical products. They explain, for example, the promise of a quantum computer exactly solving the Schrödinger equation for the caffeine molecule, limited currently by quantum hardware and its noise. They provide a background on the hardware development of quantum computers, beginning with a nuclear magnetic resonance system in 2001.

Durand, *et al.*[5] applied a quantum algorithm for economic predictive control of a chemical process including an economic model. The quantum algorithm they use is Grover's Search

Algorithm.[6] Another work on quantum computing in industrial process systems was done by You, *et al.* of Cornell University.[7]

Other authors[8,9] have used field programmable gate arrays (FPGAs) to emulate quantum circuits for modeling chemical phenomena. While one cannot execute quantum algorithms on classical structures in their natural time, FPGAs can be used to emulate quantum circuits and understand their potential speedups.

There currently exist a number of quantum algorithms for solving linear systems of equations,[10] the most prominent of which is Harrow, Hassidim and Lloyd (HHL).[11] Linear systems are fundamental in chemical kinetics,[12] partial differential equations,[13] back-propagation in neural networks,[14] and graph theory analytics.[15–17] So, the importance of a quantum speedup for solving linear systems cannot be understated.

Additionally, there are limitations to the accuracy of the approximate numerical solution provided by HHL.[10,18] Previous efforts have been made toward obtaining accurate solutions to quantum linear systems arising from chemical kinetics models.[19] One factor that was shown to influence the accuracy of HHL was the condition number of A (the ratio of the largest magnitude eigenvalue to the smallest magnitude eigenvalue of the matrix). Furthermore, preconditioners that restrict the condition number of A were previously known to be able to optimize for speed and accuracy.[18]

This work searches deeper in quantum accuracy and shows that the condition number of A is not the only control of accuracy. Many random linear systems were solved with the HHL algorithm as simulated by a Qiskit circuit. This extensive testing pinpointed a new criterion for linear systems to be accurately solved by

[a]Institute for Artificial Intelligence and Data Science, The State University of New York at Buffalo, 14260, USA

[b]Data Intensive Studies Center, Tufts University, Medford, MA 02155, USA

[c]Department of Mathematics, Tufts University, Medford, MA 02155, USA

[d]Sandia National Laboratories, Livermore, CA 94551, USA

[e]Department of Chemical and Biological Engineering, The State University of New York at Buffalo, 14260, USA. E-mail: ericwalk@buffalo.edu; Tel: +1 716 645 2909

[f]Linde Plc, 175 E Park Dr, Tonawanda, NY 14150, USA

† Electronic supplementary information (ESI) available: Table of Jacobian values, Table of RHS values, table of initial state vector values, various figures showing fidelity of quantum solution. See https://doi.org/10.1039/d2dd00049k

a quantum computer. 2 versions of a reduced hydrogen-air combustion model were accurately solved by HHL with Qiskit circuit simulations that leveraged this new criterion. The criterion for high accuracy is that the angle between the true solution and the RHS vector is very small. TChem[20] was used to compute the parameters for a Jacobian linearized model that solves for the steady state behavior of this reacting mixture. However, the full kinetic model has 9 species with 19 reversible reaction steps, and HHL can only guarantee a speedup if the linear system satisfies 4 strict criteria.[18]

The direction of this work is important because UQ encounters scaling problems which could be greatly alleviated by a quantum speedup. In particular, combustion models are known for high-dimensionality and strong non-linearity, both of which are challenging for effective UQ. While the examples presented are modest, the insights gained are critical for scaling up to larger applications of quantum computing to UQ. Furthermore, UQ is an entire field of its own,[21] with many applications in the physical sciences.[22] So, a quantum computing framework for UQ would have broad impact.

In the following sections, classical and quantum linear solvers are compared, a hydrogen-air combustion mechanism is outlined, preparation of a Jacobian linearized model is detailed, and methods for reducing the model are described. Subsequently, the results of many experiments with the Qiskit quantum circuit simulator are presented. For an accurate HHL solve, these experiments determined that the angle between the true solution and the RHS vector must be very small. Finally, this insight is leveraged for a combustion application, and directions for future work are discussed. All codes and data associated with this paper are hosted here: **https://bitbucket.org/ericawalk/quantumcombustion/src/main/**
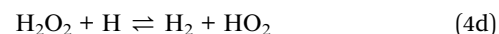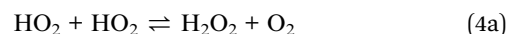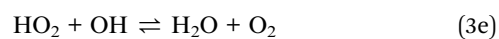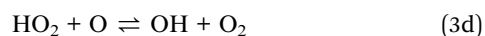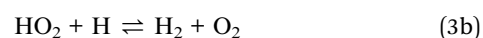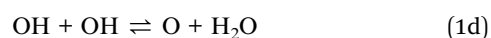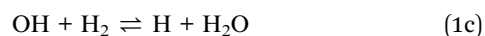
Classical and quantum linear solvers

The fastest classical linear solver runs in $O(N\kappa)$ where N is the dimension of A and κ is the condition number of A. A runtime of $O(N\sqrt{\kappa})$ can be achieved with this algorithm for any positive semidefinite matrix A. Similar to HHL, this classical algorithm can only provide an approximation of the solution vector x. For comparison, Gaussian elimination can provide the exact solution vector x in $O(N^3)$ time (unless precision is lost due to floating point error). When considering precision, ε, the computational complexity becomes $O(N\kappa \log(1/\varepsilon))$.

When certain criteria are met (which are discussed in the following section), a runtime of $O(\kappa^2 \log(N)1/\varepsilon)$ can be achieved with HHL. Certain advancements made by Ambainis[23] as well as Childs, Kothari, and Somma[24] can provide improvements in terms of the accuracy and condition number scaling, but not the scaling with respect to dimension. The runtime of HHL for systems with sparse matrices A (reaching $O(\kappa \log^3 \kappa \log N/\varepsilon^3)$ and $O(\kappa^2 \log N \log(1/\varepsilon))$, respectively).[24,25] Additionally, Wossnig, Zhao, and Prakash[27] have provided a quantum linear solver for systems with dense matrices A that runs in $O(\sqrt{N}\kappa^2 \log N/\varepsilon)$ time. In comparison, HHL is only capable of solving systems with dense matrices A in $O(N\kappa^2 \log N/\varepsilon)$ time.

Hydrogen-air combustion mechanism

For this context, we consider a system with 9 species and 19 reversible reactions as outlined by Yetter, et al.[26] for the H_2/O_2 sub-mechanism with Ar. Here, Ar is inert and does not react, distinct from air. Air contains N_2, which reacts with O_2 to form NO_x.[27] For this mechanism, the reaction equations involved in H_2–O_2 chain reactions are shown in eqn (1a)–(1d). The reaction equations involved in H_2–O_2 dissociation and recombination are shown in eqn (2a)–(2d). The reaction equations involved in the formation and consumption of HO_2 are shown in eqn (3a)–(3e). The reaction equations involved in the formation and consumption of H_2O_2 are shown in eqn (4a)–(4f).

$$H + O2 \rightleftharpoons O + OH \tag{1a}$$

$$O + H_2 \rightleftharpoons H + OH \tag{1b}$$

$$OH + H_2 \rightleftharpoons H + H_2O \tag{1c}$$

$$OH + OH \rightleftharpoons O + H_2O \tag{1d}$$

$$H_2 \rightleftharpoons H + H \tag{2a}$$

$$O + O \rightleftharpoons O_2 \tag{2b}$$

$$O + H \rightleftharpoons OH \tag{2c}$$

$$H + OH \rightleftharpoons H_2O \tag{2d}$$

$$H + O_2 \rightleftharpoons HO_2 \tag{3a}$$

$$HO_2 + H \rightleftharpoons H_2 + O_2 \tag{3b}$$

$$HO_2 + H \rightleftharpoons OH + OH \tag{3c}$$

$$HO_2 + O \rightleftharpoons OH + O_2 \tag{3d}$$

$$HO_2 + OH \rightleftharpoons H_2O + O_2 \tag{3e}$$

$$HO_2 + HO_2 \rightleftharpoons H_2O_2 + O_2 \tag{4a}$$

$$H_2O_2 \rightleftharpoons OH + OH \tag{4b}$$

$$H_2O_2 + H \rightleftharpoons H_2O + OH \tag{4c}$$

$$H_2O_2 + H \rightleftharpoons H_2 + HO_2 \tag{4d}$$

$$H_2O_2 + O \rightleftharpoons OH + HO_2 \tag{4e}$$

$$H_2O_2 + OH \rightleftharpoons H_2O + HO_2 \tag{4f}$$

Jacobian linearized ODE model

The chemical reactions in eqn (1a)–(4f) can be used to derive a first-order ordinary differential equation (ODE) model $f = \dfrac{d\boldsymbol{\theta}}{dt}$ that relates the change in each species mass fraction (θ_i) with

the reaction rates (k_i).[28–30] All of the species mass fractions can be denoted with a vector $\boldsymbol{\theta}$. Previously, a linear approximation of ordinary differential equations employed additional model constraints to remove nonlinearity.[12] Here, we use a Jacobian linearization approach to approximate the steady-state solution.

Given a vector of initial species mass fractions $\boldsymbol{\theta}_0$, TChem[20] was utilized to compute the Jacobian $\boldsymbol{J}_0$ and the RHS $\boldsymbol{f}_0$ for a Jacobian linearized model of a 0-dimensional homogenous gas reactor. Constant pressure was assumed. The entries of $\boldsymbol{J}_0, \boldsymbol{f}_0$, and $\boldsymbol{\theta}_0$ for the mechanism outlined in eqn (1a)–(4f) are shown in Table S1, Table S2, and Table S3,† respectively. The approximate equality ($\approx$) in eqn (5) and (6) arises due to the linearization method (it is like a Taylor series truncated after the first-order).

$$f \approx f_0 + J_0(\boldsymbol{\theta} - \boldsymbol{\theta}_0) \tag{5}$$

To solve eqn (5) for the steady state solution, we set $f = 0$. After a re-arrangement, we arrive at eqn (6) (which is a linear system $\boldsymbol{Ax} = \boldsymbol{b}$).

$$J_0\boldsymbol{\theta} \approx J_0\boldsymbol{\theta}_0 - f_0 \tag{6}$$

Reduced models

$H_2/O_2/Ar$ model

$$\frac{d\theta_{O_2}}{dt} = -k_{-6}\theta_{O_2} - k_{-10}\theta_{O_2}\theta_{H_2} \tag{7a}$$

$$-\frac{d\theta_{H_2}}{dt} = k_5\theta_{H_2} + k_{-10}\theta_{O_2}\theta_{H_2} \tag{7b}$$

This scenario above is known as a reduced kinetic model.[19,31] In eqn (7a) and (7b), two reacting species and one inert species are modeled. H_2 association is connected with the rate constant k_5, and O_2 dissociation is connected with the rate constant k_{-6}. Eqn (3b) has the reverse rate constant k_{-10}. The dimension of the model is 2 and the initial conditions are $\theta_{Ar} = 0.5$, $\theta_{O_2} = 0.45$, $\theta_{H_2} = 0.05$.

One constraint is that θ_{Ar} is treated as constant. θ_{H_2} and θ_{O_2} can change, but an additional constraint is that they sum to a constant overall mass balance ($\theta_{H_2} + \theta_{O_2} = 0.5$). This is represented by the first row of eqn (8a). The second row of eqn (8a) essentially represents the $d\theta_{tot}/dt$, which has been assumed to be zero. At the initial time, this would be a good approximation to the overall mechanism because all other species are zero. At steady state, however, it is not necessarily realistic. However, the answer will still balance H_2 and O_2.

$$\begin{bmatrix} 1 & 1 \\ k_5\theta_{Ar} + k_{-10}\theta_{O_2} & -k_{-6}\theta_{Ar} - k_{-10}\theta_{H_2} \end{bmatrix} \begin{bmatrix} \theta_{H_2} \\ \theta_{O_2} \end{bmatrix} = \begin{bmatrix} 0.5 \\ 0 \end{bmatrix} \tag{8a}$$

Values inside the matrix in eqn (8a) can be retrieved from the Jacobian $\boldsymbol{J}_0$. Below, this is illustrated by eqn (8b):

$$\begin{bmatrix} 1 & 1 \\ \frac{\partial}{\partial\theta_{H_2}}\left(\frac{d\theta_{H_2}}{dt}\right) & -\frac{\partial}{\partial\theta_{O_2}}\left(\frac{d\theta_{O_2}}{dt}\right) \end{bmatrix} \begin{bmatrix} \theta_{H_2} \\ \theta_{O_2} \end{bmatrix} = \begin{bmatrix} 0.5 \\ 0 \end{bmatrix} \tag{8b}$$

The classical and quantum solutions to eqn (8b) are shown in Table 1.

$H_2/O_2/H_2O/Ar$ model

Another reduced kinetic model is elaborated below. The dimension is 4 and the initial conditions are the same as above. Once again, θ_{Ar} cannot change. This is represented by the last row of eqn (9). θ_{H_2}, θ_{O_2}, and θ_{H_2O} can change, but they sum to a constant overall mass balance ($\theta_{H_2} + \theta_{O_2} + \theta_{H_2O} = 0.5$). This is represented by the third row of eqn (9a). The first and second rows of eqn (9a) correspond to $d\theta_{H_2}/dt$ and $d\theta_{O_2}/dt$, respectively. k_{-13} corresponds to the reverse rate constant of chemical eqn (3e).

$$\begin{bmatrix} 0 & k_{-10}\theta_{H_2} & 0 & k_5\theta_{H_2} \\ k_{-10}\theta_{O_2} & 0 & k_{-13}\theta_{O_2} & k_{-6}\theta_{O_2} \\ 1 & 1 & 1 & 0 \\ 0 & 0 & 0 & 1 \end{bmatrix} \begin{bmatrix} \theta_{H_2} \\ \theta_{O_2} \\ \theta_{H_2O} \\ \theta_{Ar} \end{bmatrix} = \begin{bmatrix} 0 \\ 0 \\ 0.5 \\ 0.5 \end{bmatrix} \tag{9a}$$

Values inside the matrix in eqn (9a) can be retrieved from the Jacobian $\boldsymbol{J}_0$. Below, this is illustrated by eqn (9b):

$$\begin{bmatrix} 0 & \frac{\partial}{\partial\theta_{O_2}}\left(\frac{d\theta_{H_2}}{dt}\right) & 0 & \frac{\partial}{\partial\theta_{Ar}}\left(\frac{d\theta_{H_2}}{dt}\right) \\ \frac{\partial}{\partial\theta_{H_2}}\left(\frac{d\theta_{O_2}}{dt}\right) & 0 & \frac{\partial}{\partial\theta_{H_2O}}\left(\frac{d\theta_{O_2}}{dt}\right) & \frac{\partial}{\partial\theta_{Ar}}\left(\frac{d\theta_{O_2}}{dt}\right) \\ 1 & 1 & 1 & 0 \\ 0 & 0 & 0 & 1 \end{bmatrix}$$

$$\times \begin{bmatrix} \theta_{H_2} \\ \theta_{O_2} \\ \theta_{H_2O} \\ \theta_{Ar} \end{bmatrix}$$

$$= \begin{bmatrix} 0 \\ 0 \\ 0.5 \\ 0.5 \end{bmatrix}$$

$$\tag{9b}$$

Table 1 $H_2/O_2/Ar$ model results

	θ_{H_2}	θ_{O_2}
Classical	0.356	0.144
Quantum	0.491	0.009
Preconditioned quantum	0.354	0.146

The classical and quantum solutions to eqn (9b) are shown in Table 2.

Results of numerical HHL experiments

Condition number

What follows is a demonstration using an example calculation of why the condition number of a matrix is important for accuracy and why it is related to the number of qubits in the (compute) register. A subroutine that obtains eigenvalues of the matrix A in the HHL algorithm is quantum phase estimation (QPE).[6,32–34] QPE requires that A is exponentiated as $\exp(2\pi iA)$. The purpose is to create a unitary gate. This transformation exponentiates the eigenvalues.

One consequence of the above transformation is that a large condition number will require small intervals. This is because the precision of stored eigenvalues which can be stored is $\frac{1}{2^t}$, where t is the number of qubits in the (compute) register. The number of values that can be stored doubles with every qubit, and the t qubits store the eigenvalues around the complex unit circle.

Fig. 1 illustrates eigenvalues on 1/8th intervals in the complex unit circle and off 1/8th intervals. By inference, the 1/8th intervals correspond to $t = 3$ qubits. A QPE circuit is run, and the results visualized. The matrix with the eigenvalues on the 1/8th intervals has a precise and accurate solution, but the matrix with the off-interval eigenvalues does not. QPE is a subroutine of HHL. In Fig. 1, parts (a) and (c) have the matrix,

$$CU = \begin{bmatrix} 1 & 0 \\ 0 & e^{i\pi} \end{bmatrix} \quad (10)$$

Parts (b) and (d) have the matrix:

$$CU = \begin{bmatrix} 1 & 0 \\ 0 & e^{\frac{i\pi}{3}} \end{bmatrix} \quad (11)$$

The respective shots histograms from statistical sampling of the quantum circuit are shown in parts (c) and (d). The height of a bitstring value is a probability mass. CU is the controlled unitary gate fed to the QPE for extracting eigenvalues.

Table 2 $H_2/O_2/H_2O/Ar$ model results

	θ_{H_2}	θ_{O_2}	θ_{H_2O}	θ_{Ar}
Classical	0.054	0.151	0.295	0.500
Quantum	0.000	−0.015	0.583	0.421
Preconditioned quantum	−0.032	0.168	0.304	0.553

Orthogonal tests

Orthogonal tests begin the series of tests searching for a criterion that controls the accuracy in quantum circuits solving linear systems. A Qiskit quantum circuit was used to simulate the HHL algorithm. The exact quantum state is revealed rather than the statistical shots which will be done on a real quantum computer.

A computational experiment was performed by beginning with the identity matrix and rotating the second row vector by increments of $\frac{\pi}{16}$ radians. Each system was solved with HHL as simulated by Qiskit. The accuracy of each simulation was evaluated using Qiskit's built-in metric: fidelity. The end results are shown in Fig. S1.† Fidelity is a measure of accuracy using the classical solution as a reference. Fidelity is the squared overlap between two quantum states. The classical analogy is the norm of the dot product of two vertical vectors. For these 2×2 matrices, the classical solution is expected to be accurate to machine precision. For each system, the vector b was $\frac{1}{\sqrt{2}}[1 \quad 1]^T$.

In (a), the first row of each matrix A was the vector $[1 \quad 0]$ and the second row of each matrix A was a rotation of this vector by some angle θ (in increments of $\frac{\pi}{16}$ radians). For the blue points in (b), the first row of each matrix A was the vector $[1 \quad 0]$ and the second row of each matrix A was a rotation of this vector by some angle θ (increments of $\frac{\pi}{16}$ radians) but over a different domain than part (a). For the red points in (b), these rows are permuted. In other words, the first row and the second row are swapped. Thus, even though the blue and red points correspond to the same set of select linear systems of equations, the blue points use the diagonally dominant representation while the red points do not. These results appear to show that the closer to orthogonal a matrix is, the greater the accuracy obtained with HHL. However, these results are not proof, which is why the next test is conducted.

To further interrogate the orthogonality criterion for quantum accuracy, random orthogonal matrices were evaluated. Random orthogonal Q matrices were obtained from the QR decomposition of random matrices. The entries of the random matrices are random numbers over the interval $[0,1)$ with a uniform probability distribution. The results are shown in Fig. S2.† In (a), each system has the vector $b = \frac{1}{\sqrt{2}}[1 \quad 1]^T$ and each random orthogonal matrix A is 2 by 2. In (b), each system has the vector $b = \frac{1}{2}[1 \quad 1 \quad 1 \quad 1]^T$ and each random orthogonal matrix A is 4 by 4. The results from Fig. S2† reveal that when the input matrix is perfectly orthogonal, HHL is not accurate.

Orthonormal tests

It could be that the requirement for accuracy is that the vectors of the matrix be orthonormal. That is, beyond orthogonality, tested with negative results above, it could be necessary that
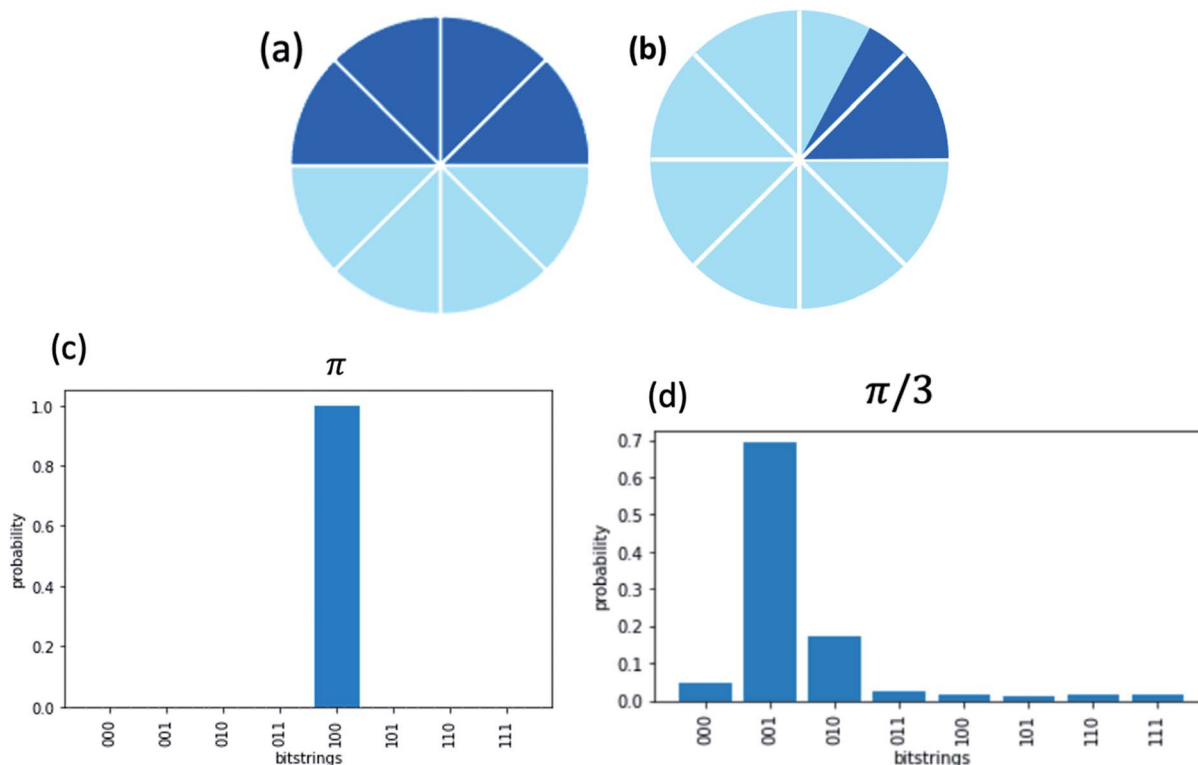
Fig. 1 Quantum phase estimation (QPE) depends upon the condition number of the matrix. Eigenvalues will be placed on the complex unit circle. If the condition number, or ratio of largest to smallest eigenvalue is large, more qubits must be used to obtain smaller precision slices. (a) One half eigenvalue placed in the controlled unitary matrix. (b) One-sixth eigenvalue. (c) Precise readout from one half eigenvalue. (d) Imprecise readout due to not laying on an allowed interval.

those vectors also have unit length. So, in order to obtain the random orthonormal matrices used in this computational experiment, the Q matrices from the QR decomposition of random matrices were normalized by scaling the rows to be unit length. The results are shown in Fig. S3.† For two-dimensional systems with orthonormal matrices, the vector $b = \frac{1}{\sqrt{2}}[1 \quad 1]^T$ and each random orthonormal matrix A is 2 by 2. Random orthonormal tests did not yield accurate quantum solutions.

Diagonal tests

Diagonal matrices were constructed with random numbers on the diagonal from a uniform probability distribution over the interval [0, 1]. Off-diagonal entries were set to zero. The results from the quantum accuracy tests are shown in Fig. S4.† In (a), each system has the vector $b = \frac{1}{\sqrt{2}}[1 \quad 1]^T$ and each random diagonal matrix A is 2 by 2. In (b), each system has the vector $b = \frac{1}{2}[1 \quad 1 \quad 1 \quad 1]^T$ and each random diagonal matrix A is 4 by 4. These systems with random diagonal matrices exhibited higher accuracy, broadly speaking, than the ones with random orthogonal matrices. Still the accuracy is less than acceptable for UQ studies.

Angle of the true solution with the RHS vector

A foundational linear algebra principle of matrices is the concept of eigendecomposition. An interrogation of quantum accuracy criterion of linear systems would be incomplete without considering eigenvalues and eigenvectors. The eigendecomposition equation is:

$$Av = \lambda v \tag{12}$$

The eigenvector is v and its corresponding eigenvalue is λ. In the case where the RHS of eqn (12) is a linear multiplier of the solution vector, v. The angle between v and λv is necessarily zero. The potential of this small angle for high accuracy solutions was hinted at by the high fidelity solution for angle zero in previous tests.

It was observed that higher accuracy with HHL was consistent with a smaller angle between the classical solution x and the vector b. This angle θ is shown on the x-axes in Fig. 2 and 3. In Fig. 2, each system has the vector $b = \frac{1}{\sqrt{2}}[1 \quad 1]^T$ and each random diagonal matrix A is 2 by 2. The outlier at the low angle in Fig. 2 is likely due to using a limited number of qubits in simulating the quantum circuit with an HHL algorithm. In

Fig. 3, each system has the vector $\boldsymbol{b} = \frac{1}{2}\begin{bmatrix} 1 & 1 & 1 & 1 \end{bmatrix}^T$ and each random diagonal matrix $\boldsymbol{A}$ is 4 by 4.

When $\theta = 0$, near perfect accuracy can be obtained with HHL. One such case of when $\theta = 0$ is when the system is $\boldsymbol{Ax} = \lambda\boldsymbol{v}$ for some eigenvalue λ and eigenvector $\boldsymbol{v}$ pair of $\boldsymbol{A}$. This is shown in Fig. S5.† In (a), each matrix $\boldsymbol{A}$ is 2 by 2. In (b), each matrix $\boldsymbol{A}$ is 4 by 4. Another such case of when $\theta = 0$ is when the system is $\boldsymbol{Ax} = \boldsymbol{v}$ for some eigenvector $\boldsymbol{v}$ of $\boldsymbol{A}$. This is shown in Fig. S6.† In (a), each matrix $\boldsymbol{A}$ is 2 by 2 and the vector $\boldsymbol{b} = \begin{bmatrix} 1 & 0 \end{bmatrix}^T$ is an eigenvector of $\boldsymbol{A}$. In (b), each matrix $\boldsymbol{A}$ is 4 by 4 and the vector $\boldsymbol{b} = \begin{bmatrix} 1 & 0 & 0 & 0 \end{bmatrix}^T$ is an eigenvector of $\boldsymbol{A}$. Creating this eigenvector is done by filling the first column with zeroes starting on the second row. Most generally, $\theta = 0$ when $\boldsymbol{b}$ is any nonzero scalar multiple of an eigenvector of $\boldsymbol{A}$. In this equation, λ and $\boldsymbol{v}$ are some eigenvalue and eigenvector pair of $\boldsymbol{A}$. c can be any nonzero scalar.

$$\boldsymbol{Ax} = (c\lambda)\boldsymbol{v} \tag{13}$$

The solution to this linear system is $\boldsymbol{x} = c\boldsymbol{v}$. Thus, $\boldsymbol{xb} = 1$ and $\cos^{-1}(1) = 0$. Empirically, it has been seen in Fig. S1† that it is possible for $\theta = 0$ when $\boldsymbol{b}$ is a linear combination of the eigenvectors of $\boldsymbol{A}$. In this case, when the fidelity (accuracy) has peaked, the RHS vector can be written as an equal contribution of each of the two eigenvectors.

$$\frac{1}{\sqrt{2}}\begin{bmatrix} 1 \\ 1 \end{bmatrix} = \frac{1}{\sqrt{2}}\begin{bmatrix} 1 \\ 0 \end{bmatrix} + \frac{1}{\sqrt{2}}\begin{bmatrix} 0 \\ 1 \end{bmatrix} \tag{14}$$

So, given a sufficient number of qubits for the condition number of the matrix, the key criterion for an accurate HHL solve is that the angle between the true solution with the RHS vector is very small. For practical scientific and engineering applications, this implies that most systems will have to be preconditioned to meet this criterion. In the next section, one
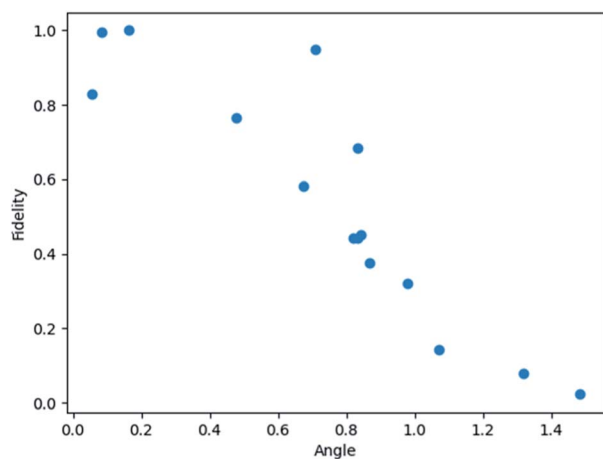

Fig. 3   Fidelity of quantum solution to linear systems of equations ($\boldsymbol{Ax} = \boldsymbol{b}$) with random 4 by 4 matrices $\boldsymbol{A}$. On the x-axis, the angle shown is between the true solution $\boldsymbol{x}$ and the RHS $\boldsymbol{b}$.

way of preconditioning for this criterion is presented and applied to 2 reduced models of hydrogen-air combustion.

Results of combustion application

Combustion models

For the $H_2/O_2/Ar$ model, eqn (8b) can be preconditioned with a 2D rotation matrix to maximize its accuracy. Due to both sides of the equations being multiplied by the rotation matrix, the $\boldsymbol{x}$ solution vector remains constant, while the RHS vector, $\boldsymbol{b}$, is rotated.

$$\begin{bmatrix} \cos\phi & -\sin\phi \\ \sin\phi & \cos\phi \end{bmatrix} \begin{bmatrix} 1 & 1 \\ \frac{\partial}{\partial\theta_{H_2}}\left(\frac{d\theta_{H_2}}{dt}\right) & -\frac{\partial}{\partial\theta_{O_2}}\left(\frac{d\theta_{O_2}}{dt}\right) \end{bmatrix} \begin{bmatrix} \theta_{H_2} \\ \theta_{O_2} \end{bmatrix}$$
$$= \begin{bmatrix} \cos\phi & -\sin\phi \\ \sin\phi & \cos\phi \end{bmatrix} \begin{bmatrix} 0.5 \\ 0 \end{bmatrix} \tag{15}$$

For this model, a rotation angle of $\phi = \frac{\pi}{8}$ radians was used. This transformation makes the angle between the exact solution $\boldsymbol{x}$ and the RHS vector $\boldsymbol{b}$ less than 0.01 radians. After preconditioning, the HHL solution exhibits perfect accuracy (see Table 1). Further evidence of the small angle yielding an accurate quantum solution will be seen in the four-dimensional combustion model below. This new preconditioning method will greatly increase the cost of solving one linear system with HHL. However, in the context of UQ, this cost could be offset by leveraging the ability to apply one optimal preconditioner to many samples of the forward model.

The $H_2/O_2/H_2O/Ar$ model can be preconditioned using a product of 4D rotation matrices,

Fig. 2   Fidelity of quantum solution to linear systems of equations ($\boldsymbol{Ax} = \boldsymbol{b}$) with random 2 by 2 matrices $\boldsymbol{A}$. On the x-axis, the angle shown is between the true solution $\boldsymbol{x}$ and the RHS $\boldsymbol{b}$.

$$P(\phi) = \begin{bmatrix} \cos\phi_3 & 0 & 0 & -\sin\phi_3 \\ 0 & \cos\phi_4 & -\sin\phi_4 & 0 \\ 0 & \sin\phi_4 & \cos\phi_4 & 0 \\ \sin\phi_3 & 0 & 0 & \cos\phi_3 \end{bmatrix}$$

$$\times \begin{bmatrix} \cos\phi_2 & 0 & -\sin\phi_2 & 0 \\ 0 & \cos\phi_5 & 0 & -\sin\phi_5 \\ \sin\phi_2 & 0 & \cos\phi_2 & 0 \\ 0 & \sin\phi_5 & 0 & \cos\phi_5 \end{bmatrix}$$

$$\times \begin{bmatrix} \cos\phi_1 & -\sin\phi_1 & 0 & 0 \\ \sin\phi_1 & \cos\phi_1 & 0 & 0 \\ 0 & 0 & \cos\phi_6 & -\sin\phi_6 \\ 0 & 0 & \sin\phi_6 & \cos\phi_6 \end{bmatrix} \quad (16)$$

For this model, rotation angles of $\phi_1 = 0$ radians, $\phi_2 = \frac{13\pi}{8}$ radians, $\phi_3 = \frac{10\pi}{8}$ radians, $\phi_4 = \frac{9\pi}{8}$ radians, $\phi_5 = \frac{7\pi}{8}$ radians, and $\phi_6 = \frac{14\pi}{8}$ radians were used. This transformation makes the angle between the exact solution x and the vector b less than 0.06 radians. The results for the HHL quantum solution for this preconditioned system are presented in Table 2, along with the classical solution.

Conclusions

This paper identified a key criterion necessary for the accurate solution of linear systems of equations with HHL, which is a key element for incorporating this quantum algorithm into scientific computing. The criterion is that the angle between the solution vector and the RHS vector is small. A preconditioner in the form of a product of rotation matrices can optimize for this criterion. This method could be applied to any application of HHL. Therefore, the potential for cross-domain impact is vast.

Using Qiskit to emulate an HHL circuit, we demonstrate the preparation and application of optimal preconditioners for obtaining accurate steady state solutions to simplified hydrogen-oxygen combustion models with 2 and 4 species.

In the context of UQ problems, we hypothesize that a single optimal preconditioner can be found once for the mean sample. Then, the same matrix could be used to precondition all samples. This way, quantum speedup could be maintained. Future work can test the accuracy of applying one optimized preconditioner to all samples. It is likely that this method has limitations to the amount of perturbation with a still-acceptable accuracy.

Future work also includes extracting statistics (namely mean and variance) pertaining to the entries of the quantum state containing the solutions to all of the samples. An oft-cited criticism of HHL is that the number of shots necessary to statistically extract the solution vector x is so large that it could cancel out a scaling advantage. However, UQ problems do not require knowing all entries of x; they only require information such as the mean or variance of x. So, if additional gate operations can be performed on x to prepare these statistics, then perhaps HHL can retain a quantum advantage in UQ applications.

Ultimately, this article is another small but necessary step on the path to achieving "quantum supremacy" in the area of UQ.

Data availability

All codes and data associated with this paper and the data that support the findings of this study will be made openly available upon publication at in **https://bitbucket.org/ericawalk/quantumcombustion/src/main/**.

Conflicts of interest

There are no conflicts to declare.

Acknowledgements

References

1 National Academies of Sciences, *E.; Medicine, Quantum Computing: Progress and Prospects*, The National Academies Press, Washington, DC, 2019, p. 272.

2 P. W. Shor, in Algorithms for Quantum Computation: Discrete Logarithms and Factoring, *Proceedings 35th Annual Symposium on Foundations of Computer Science*, vol. 20–22, Nov. 1994, pp. 124–134.

3 J. Biamonte, P. Wittek, N. Pancotti, P. Rebentrost, N. Wiebe and S. Lloyd, Quantum Machine Learning, *Nature*, 2017, **549**, 195–202.

4 M. P. Andersson, M. N. Jones, K. V. Mikkelsen, F. You and S. S. Mansouri, Quantum Computing for Chemical and Biomolecular Product Design, *Curr. Opinion Chem. Eng.*, 2022, **36**, 100754.

5 K. Nieman, K. K. Rangan and H. Durand, On Probabilistic Input Selection: Utilizing a Quantum Algorithm in Selecting Inputs for Lyapunov-Based Economic Model Predictive Control Formulated as a Look-up Table, in *American Institute of Chemical Engineers Annual Meeting*, ed. M. Ellis, AIChE, Boston, MA, 2021.

6 J. D. Hidary, *Quantum Computing: An Applied Approach*, Springer International Publishing, 2019, XIX, p. 379.

7 A. Ajagekar and F. You, Quantum Computing Assisted Deep Learning for Fault Detection and Diagnosis in Industrial Process Systems, *Comput. Chem. Eng.*, 2020, **143**, 107119.

8 J. Pilch and J. Długopolski, An FPGA-Based Real Quantum Computer Emulator, *J. Comput. Electron.*, 2019, **18**, 329–342.

9 J. M. Rodríguez-Borbón, A. Kalantar, S. S. R. K. C. M. Yamijala, B. Oviedo, W. Najjar and B. M. Wong, Field Programmable Gate Arrays for Enhancing the Speed and Energy Efficiency of Quantum Dynamics Simulations, *J. Chem. Theory Comput.*, 2020, **16**, 2085–2098.

10 D. Dervovic, M. Herbster, P. Mountney, S. Severini, N. Usher and L. Wossnig, *Quantum Linear Systems Algorithms: A Primer*, arXiv Quantum Physics, 2018.

11 A. W. Harrow, A. Hassidim and S. Lloyd, Quantum Algorithm for Linear Systems of Equations, *Phys. Rev. Lett.*, 2009, **103**, 150502.

12 E. A. Walker and S. A. Pallathadka, How a Quantum Computer Could Solve a Microkinetic Model, *J. Phys. Chem. Lett.*, 2021, **12**, 592–597.

13 E. Bueler, *Petsc for Partial Differential Equations: Numerical Solutions in C and Python*; SIAM, 2020, p xvi + 391.

14 R. J. Erb, Introduction to Backpropagation Neural Network, *Computation. Pharm. Res.*, 1993, **10**, 165–170.

15 E. A. Walker, M. M. Mohammadi and M. T. Swihart, Graph Theory Model of Dry Reforming of Methane Using Rh (111), *J. Phys. Chem. Lett.*, 2020, **11**, 4917–4922.

16 E. K. J. Walker, J. Goetz, M. T. Robo, A. Tewari and P. M. Zimmerman, Learning to Predict Reaction Conditions: Relationships between Solvent, Molecular Structure, and Catalyst, *J. Chem. Inf. Model.*, 2019, **59**, 3645–3654.

17 S. F. Muldoon, E. W. Bridgeford and D. S. Bassett, Small-World Propensity and Weighted Brain Networks, *Sci. Rep.*, 2016, **6**, 22057.

18 S. Aaronson, Read the Fine Print, *Nat. Phys.*, 2015, **11**, 291–293.

19 A. Becerra, A. Prabhu, M. S. Rongali, S. C. S. Velpur, B. Debusschere and E. A. Walker, How a Quantum Computer Could Quantify Uncertainty in Microkinetic Models, *J. Phys. Chem. Lett.*, 2021, **12**, 6955–6960.

20 K. Kim, O. Diaz-Ibarra, C. Safta and H. Najm, *Tchem V2.0 – a Software Toolkit for the Analysis of Complex Kinetic Models*, Sandia National Laboratories, 2020.

21 T. J. Santner, B. J. Williams and W. I. Notz, *The Design and Analysis of Computer Experiments*, Springer, 2003.

22 H. N. Najm, B. J. Debusschere, Y. M. Marzouk, S. Widmer and O. P. Le Maître, Uncertainty Quantification in Chemical Systems, *Int. J. Numer. Methods Eng.*, 2009, **80**, 789–814.

23 A. Ambainis, *Variable Time Amplitude Amplification and a Faster Quantum Algorithm for Solving Systems of Linear Equations*, arXiv- quant-ph, 2010.

24 A. M. Childs, R. Kothari and R. D. Somma, Quantum Algorithm for Systems of Linear Equations with Exponentially Improved Dependence on Precision, *SIAM J. Comput.*, 2017, **46**, 1920–1950.

25 L. Wossnig, Z. Zhao and A. Prakash, Quantum Linear System Algorithm for Dense Matrices, *Phys. Rev. Lett.*, 2018, **120**, 050502.

26 R. A. Yetter, F. L. Dryer and H. Rabitz, A Comprehensive Reaction Mechanism for Carbon Monoxide/Hydrogen/Oxygen Kinetics, *Combust. Sci. Technol.*, 1991, **79**, 97–128.

27 C.-H. Liu, K. Giewont, T. J. Toops, E. A. Walker, C. Horvatits and E. A. Kyriakidou, Non-Catalytic Gas Phase No Oxidation in the Presence of Decane, *Fuel*, 2021, **286**, 119388.

28 K. Giewont, E. A. Kyriakidou and E. A. Walker, Investigation of Potential Catalytic Active Sites of Pd/SSZ-13: A DFT Perspective, *J. Phys. Chem. C*, 2021, **125**(28), 15262–15274.

29 A. Savara and E. Walker, Chekipeuq Intro 1: Bayesian Parameter Estimation Considering Uncertainty or Error from Both Experiments and Theory, *ChemCatChem*, 2020, **12**(21), 5385–5400.

30 S. Matera, W. F. Schneider, A. Heyden and A. Savara, Progress in Accurate Chemical Kinetic Modeling, Simulations, and Parameter Estimation for Heterogeneous Catalysis, *ACS Catal.*, 2019, **9**, 6624–6647.

31 E. A. Walker, K. Ravisankar and A. Savara, Chekipeuq Intro 2: Harnessing Uncertainties from Data Sets, Bayesian Design of Experiments in Chemical Kinetics, *ChemCatChem*, 2020, **12**, 5401–5410.

32 G. M. D'Ariano, C. Macchiavello and M. F. Sacchi, On the General Problem of Quantum Phase Estimation, *Phys. Lett. A*, 1998, **248**, 103–108.

33 U. Dorner, R. Demkowicz-Dobrzanski, B. J. Smith, J. S. Lundeen, W. Wasilewski, K. Banaszek and I. A. Walmsley, Optimal Quantum Phase Estimation, *Phys. Rev. Lett.*, 2009, **102**, 040403.

34 T. E. O'Brien, B. Tarasinski and B. M. Terhal, Quantum Phase Estimation of Multiple Eigenvalues for Small-Scale (Noisy) Experiments, *New J. Phys.*, 2019, **21**, 023022.